View Article Online
DOI: 10.1039/D0TC03816D

ARTICLE

Thermal-induced interface degradation in perovskite light-emitting diodes

Received 00th January 20xx,
Accepted 00th January 20xx

DOI: 10.1039/x0xx00000x

Yatao Zou[a,b], Tian Wu[a], Fan Fu[c], Sai Bai[b], Lei Cai[a], Zhongcheng Yuan[b], Yajuan Li[a], Ruiying Li[a], Weidong Xu[b], Tao Song[a], Yingguo Yang[d], Xingyu Gao[d], Feng Gao[b*], Baoquan Sun[a*]*

Perovskite light-emitting diodes (PeLEDs) have experienced rapid improvements in the device efficiency during the last several years. However, the operational instability of PeLEDs remains a key barrier hindering their practical applications. A fundamental understanding of the degradation mechanism is still lacking but will be important to seek ways to mitigate these unwanted processes. In this work, through comprehensive characterizations on the perovskite emitters and the interfacial contacts, we figure out that the Joule heating induced interface degradation is one of the dominant factors affecting the operational stability of PeLEDs. We investigate the interfacial contacts of PeLEDs based on a commonly used device structure with organic electron transport layer of 1, 3, 5-tris (N-phenylbenzimiazole-2-yl) benzene (TPBi), and observe obvious photoluminescence quenching of the perovskite layer after device operation. Detailed characterizations on the interlayers and the interfacial contacts reveal that the photoluminescence quenching is mainly ascribed to the element inter-diffusion at the interface induced by the morphological evolution of TPBi layers under Joule heating during operation of PeLEDs. Our work provides direct insight into degradation pathways and highlights the importance of exploring intrinsically stable interlayers as well as interfacial contacts beyond the state-of-the-art to further boost the operational stability of PeLEDs.

Introduction

Metal halide perovskite light-emitting diodes (PeLEDs) are rising as one of the most promising technologies for lighting and display applications, owing to their low material and processing costs, high efficiencies, and superior color purity[1-6]. Recently, with great efforts on engineering the device structures and perovskite films, peak external quantum efficiencies (EQEs) of PeLEDs with green, red, and near-infrared emission have been rapidly improved to over 20%[7-10], which are comparable with the mature light-emitting technologies based on organic semiconductors and inorganic colloidal quantum dots[11, 12]. Despite the remarkable improvements in the device efficiencies, the operational stability of the state-of-the-art PeLEDs is still far behind the requirement for further commercialization[8, 9, 13, 14]. In addition, as a young technology, degradation behaviors and the related degradation mechanisms of PeLEDs are still open, calling further investigations on both the perovskite emissive layers and the interfacial contacts.

For PeLEDs with commonly used multilayer device structures, the operational stability is highly relevant to luminescent stability of perovskite emissive layers, intrinsic material stability of charge transport layers (CTLs) as well as interfacial contacts between perovskite films and CTLs[15-18]. According to well-studied perovskite photovoltaics[19-21], ion migration in perovskite active layers, which causes the generation of trap states, the charge accumulation at the interfaces and corrosion of the metal electrodes during device operation, is also believed to be one of the intrinsic threats to the long-term operational stability of PeLEDs[22, 23]. Considering that the ion migration is a thermal-activated process, the ion movement in PeLEDs is expected to be even severer under high current density (or high driving voltage) and long-term operation, which associates with a significantly enhanced Joule heating in the devices. Previous reports have proposed several useful strategies on enhancing the operational stability of PeLEDs through optimizing the perovskite emissive layers. For example, via engineering the stoichiometric ratio of perovskite precursors and incorporating passivation agents, *i.e.* 5-aminovalleric acid, lithium bromide, to reduce the defects and mitigate the ion migration pathways, PeLEDs with enhanced operational lifetimes could be achieved[8, 18, 24-26]. Improved operational lifetime of PeLEDs through reducing the Joule heating were also demonstrated, yet a deep understanding on how the Joule heating influences the stability of PeLEDs is still lacking[27-30]. In addition to improving the stability of emitting layer of perovskites, highly stable interfacial contacts are equally critical to the operational stability. As most of the commonly used organic CTLs in PeLEDs are thermodynamically unstable[31, 32], the generated Joule heating

[a] Jiangsu Key Laboratory for Carbon-Based Functional Materials & Devices, Institute of Functional Nano & Soft Materials (FUNSOM) and Collaborative Innovation Center of Suzhou Nano Science and Technology, Soochow University, 199 Ren'ai Road, Suzhou 215123, People's Republic of China.
[b] Department of Physics, Chemistry and Biology (IFM), Linköping University, SE-581 83 Linköping, Sweden.
[c] Laboratory for Thin Films and Photovoltaics, Empa-Swiss Federal Laboratories for Materials Science and Technology, Ueberlandstrasse 129, 8600, Duebendorf, Switzerland.
[d] Shanghai Synchrotron Radiation Facility (SSRF), Shanghai Institute of Applied Physics, Chinese Academy of Sciences, 239 Zhangheng Road, Pudong New Area, Shanghai 201204, China
†Electronic Supplementary Information (ESI) available. See DOI: 10.1039/x0xx00000x

View Article Online
DOI: 10.1039/D0TC03816D

in working devices may cause irreversible change to the CTLs, resulting in detrimental effects on the interfacial contacts, the luminescent properties of perovskite films and the operational stability of PeLEDs. Recently, Wu and co-workers demonstrated an all-inorganic device architecture to improve the stability of PeLEDs, partially owing to the suppressed diffusion of metallic atoms from cathode into perovskites.[33] The notably improved device operational stability of the PeLEDs highlight the importance of rational design of the device structures, which calls further understanding of the stability of the interlayers, the interfacial contacts, and their effects on the operational stability of PeLEDs.

In this work, we demonstrate that the thermal-induced interface degradation of PeLEDs is one of the dominant factors affecting the operational stability of PeLEDs. A commonly used device structure consisting of an *n*-type organic electron transport layer (ETL) of 1, 3, 5-tris (N-phenylbenzimiazole-2-yl) (TPBi) between the perovskite and metal electrode (aluminum, Al) is investigated. Pronounced Joule heating from operating PeLEDs is observed, where the surface temperature increase to around 70 °C under a high voltage. We observe morphological change of the TPBi film under heat stress, which causes non-negligible element inter-diffusion at the interface and direct contacts between the top aluminum electrode and the perovskites, leading to obvious luminescence quenching of perovskite emissive layers. Our work clearly reveals the detrimental effects of the interfacial degradation induced by the Joule heating in working PeLEDs on the device performance and operational stability.

Results and Discussions

The investigated PeLEDs are constructed based on a commonly used positive-intrinsic-negative (p-i-n) device structure consisting of indium tin oxide (ITO) /poly (N-vinylcarbazole) (PVK) /perovskite/TPBi/lithium fluoride (LiF) /Al (Fig. 1a). Thin films of $CsPbBr_3$ with the incorporation of rational phenylethylammonium bromide (PEABr) are used as the perovskite emissive layers, which was demonstrated in previous efficient green PeLEDs[34, 35]. Fig. 1b and c show the current density-voltage-luminescence (*J-V-L*) and current efficiency-current density-EQE (*CE-J-EQE*) curves of a typical PeLED, exhibiting a maximum brightness of approximately 9,000 cd m^{-2} and a peak CE of 40.2 cd A^{-1}, corresponding to a peak EQE of 12.8%. From the *CE-J-EQE* curve, we also measure an obvious efficiency roll-off with the EQE decreases to 40% of its peak value at a current density of approximately 50 mA cm^{-2}. We further measure an operational half-lifetime (T_{50}), which is defined as the time needed to decay to 50% of its initial brightness, to be 14.2 min at an initial brightness of approximately 200 cd m^{-2} (Fig. 1d).

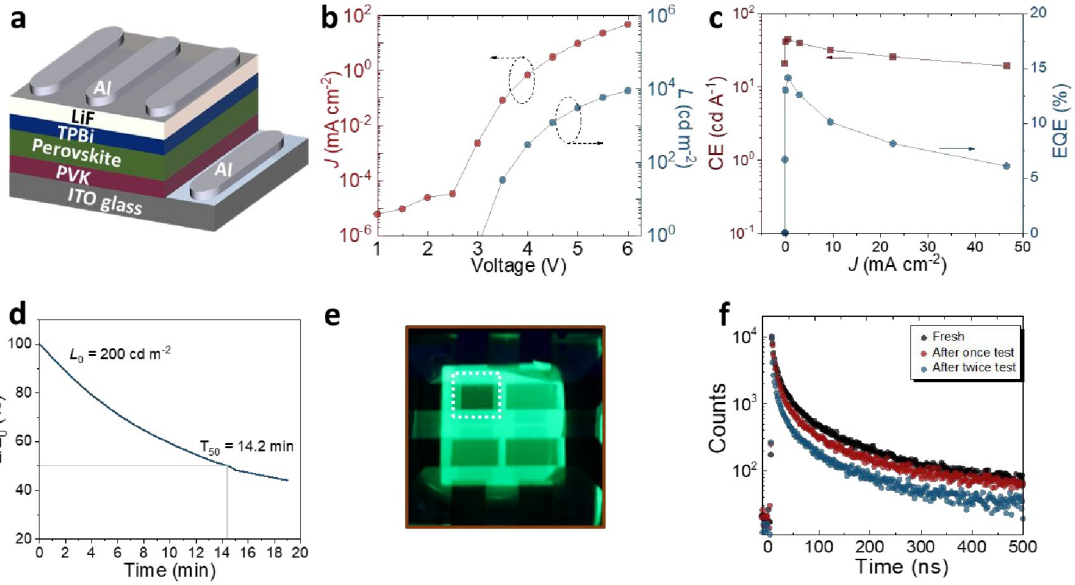

Fig.1 Device performance of a PEABr-based PeLED. (a) Schematic device structure. The thickness of each layers is not proportional to the real device. (b) *J-V-L* curve. (c) *CE-J-EQE* curve. (d) Operational lifetime measurement with an initial luminescence of 200 cd m^{-2}. (e) Photograph of PeLED under 365 nm UV lamp illumination from glass side, the pixel in white dash rectangle has been scanned from 0 to 6 V. (f) PL lifetime decay of perovskite films with different testing cycles.

View Article Online
DOI: 10.1039/D0TC03816D

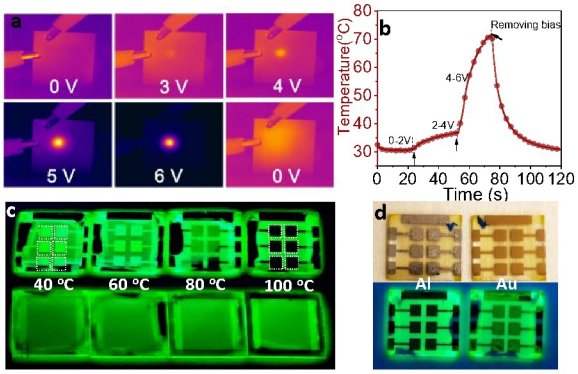

Fig. 2 Temperature evolution at ITO/glass surface of PeLEDs during bias scan from 0 to 6 V. (a) Temperature of PeLEDs operated at different bias at ITO/glass recorded by a near-infrared camera. (b) Extracted device surface temperature against time curve. (c) Photographs of a completed PeLED device and a perovskite film covered by TPBi and LiF annealed at different temperature under 365 nm UV lamp illumination. Top photographs are completed LED devices, while bottom ones are perovskite films covered with only TPBi and LiF. The dashed squares mark six active pixels of PeLEDs. (d) Photographs of perovskite films covered with only Al or Au under natural light (top) and 365 nm UV lamp (bottom), respectively.

We notice obviously decreased photoluminescence (PL) from the perovskite emissive layer of the tested pixel after a scan from 0 to 6 V (step 0.25 V), as shown in Fig. 1e. We note that the PL quenching is nonreversible, which cannot recover even after a long time relaxing after removing the applied bias, indicating a permanent damage to the perovskite films during the device measurement. We characterize decreased PL intensity and shorten PL lifetime of the perovskite emissive layer after device measurements (Fig. S1 and Fig. 1f), which is consistent with increased trap states or quench centers in the perovskite films[36, 37]. In addition, the device after two scans exhibits a significantly reduced maximum brightness of approximately 6,000 cd m^{-2} and a decreased peak EQE of 5.4% (Fig. S2). The results suggest poor stability of the PeLEDs, which is likely due to the significant PL quenching of the perovskite films under operating conditions. We also fabricate PeLEDs with another commonly used organic ETL of bis-4,6-(3,5-di-3-pyridylphenyl)-2-methylpyrimidine (B3PYMPM) and present the device performance results in Fig. S3. We observe the same PL quenching behavior (insert in Fig. S3b) of the perovskite film after device measurement and short device operational lifetime, indicating that there are intrinsic stability issues for the PeLEDs with commonly used p-i-n device structures consisting of thermally evaporated organic ETLs.

To understand the reasons for the PL quenching of the perovskite emissive layer, we first investigate if there is any change over the perovskite crystal structure after the device measurements. We present the grazing incidence X-ray diffraction (GIXRD) results of perovskite films in fresh and bias operated devices in Fig. S4. Two diffraction rings at q= 15.27 and 21.50 nm^{-1} in the GIXRD spectra can be assigned to (110) and (200) planes of cubic $CsPbBr_3$ phase[34], respectively. The integrated spectra in Fig. S4c to f show similar crystallinity and orientation of the perovskite films in fresh and scanned devices, suggesting negligible change over the crystal structure of the perovskite emissive layers after measurements.

We observe that the investigated PeLEDs generate obvious Joule heating during the device measurements. We record the surface temperature evolution during the scan from the glass side of one typical device using a near-infrared camera (Fig. 2a and b). Before turning on, the surface temperature of the device is approximately 30 °C, which is close to the room temperature. We monitor significantly increased surface temperature to over 70 °C under a bias of 6 V, corresponding to a current density of 50 mA cm^{-2}. According to the different heating diffusion coefficient and the thickness of each functional layer in the PeLEDs, we believe that the real temperature at the perovskite interface might be higher than that of the detected temperature from the glass side[38-40].

We proceed to evaluate the heating effects on the PL properties of perovskite emissive layers with different interfacial contacts. We observe clear PL quenching of the perovskite films in the overlap region between perovskite and Al electrode in the complete devices after annealing at a temperature higher than 60 °C (top images in Fig. 2c). In contrast, for the samples with only thermally evaporated TPBi and LiF on top of the perovskite films, we observe negligible PL quenching after thermal annealing at the same temperature, as shown in bottom images in Fig. 2c. The results suggest that the PL quenching of perovskite layers under heating is likely to be relevant to the Al electrode on top. To confirm this, we directly deposit the Al on top of perovskite film and anneal the samples at a relative low temperature of 60 °C for 5 min. We notice that the Al electrode becomes rough and almost no PL can be observed from the overlap region between perovskite films and Al electrode (left images in Fig. 2d), indicating possible interfacial reaction at the interface. After replacing the Al with a more stable gold (Au) electrode, PL quenching of perovskite films can be effectively suppressed under the same annealing conditions (right images in Fig. 2d). The results are consistent with previously observed perovskite decomposition due to the redox reaction between Al and perovskite films[41]. We conclude that the unrecoverable luminescent properties of perovskite films after device measurements can be mainly ascribed to direct contacts or element inter-diffusion between the Al electrode and the perovskite films in PeLEDs.

To reveal detailed information on the interface degradation in the PeLEDs under working conditions, we characterize the vertical element distribution in devices before and after biasing using time-of-flight secondary ion mass spectrometry (ToF-SIMS) measurements. This technique has been used to investigate ions diffusion process in formamidinium lead iodide based PeLEDs with an n-i-p device structure and Au electrode, and it is found that iodide dissociation from the perovskite layer accompanied by generation and migration of halide defects[42]. In the contrary, our ToF-SIMS results suggest that the degradation of PeLEDs based on the p-i-n structure is associated with direct contact between aluminum and perovskite. We present the ToF-SIMS depth profiles of fresh devices, devices after scanning from 0 to 6 V (step 0.25 V) and devices after long-term operation under constant current (degrade to 30% of its initial brightness) in Fig. 3a to 3c. The functional layer of Al, LiF, TPBi, and perovskite can be distinguished by the $CsAl^+$, F^+, C_2^+, Pb^+ signals, respectively, as depicted by the navy, green, red, and gray lines in ToF-SIMS depth profile spectra. In the fresh device, the Pb^+ signal can only be detected after the C_2^+ signal

View Article Online
DOI: 10.1039/D0TC03816D

significantly drops to a low level, indicating a distinct interface between perovskite and TPBi layer (Fig. 3a). However, for both devices scanned from 0 to 6 V and after long-term operation, ToF-SIMS depth profile suggests a mixed interface between perovskite and TPBi layer. The Pb^+ signal emerged when the C_2^+ signal remains at a high level (Fig. 3b and c). In this multilayer device without compact buffer layer on the TPBi layer, the mixed interface between perovskite and TPBi is likely to cause direct contact or serious element inter-diffusion between the Al electrode and perovskite films. This is also consistent with the ToF-SIMS results, showing the accumulation of Al ions at the perovskite interface and possibly within the perovskite active layer.

rather than the change to the perovskite film under heating, evidenced by the observed same trend in the roughness of TPBi on top of bare PVK (Fig. S5). The visible morphology change can be attributed to a low glass transition temperature of TPBi of approximately 120 °C, as revealed by the differential thermal analysis results in Fig. S6. Considering the obvious Joule heating during the device operation, we anticipate that the perovskite compositions and/or metal elements in the Al electrode may easily diffuse through the TPBi layer, which is facilitated by the morphological variation, resulting in significant PL quenching of the perovskite emissive layers.

Having revealed the detrimental effects of Joule heating induced interface degradation on the stability of PeLEDs, we

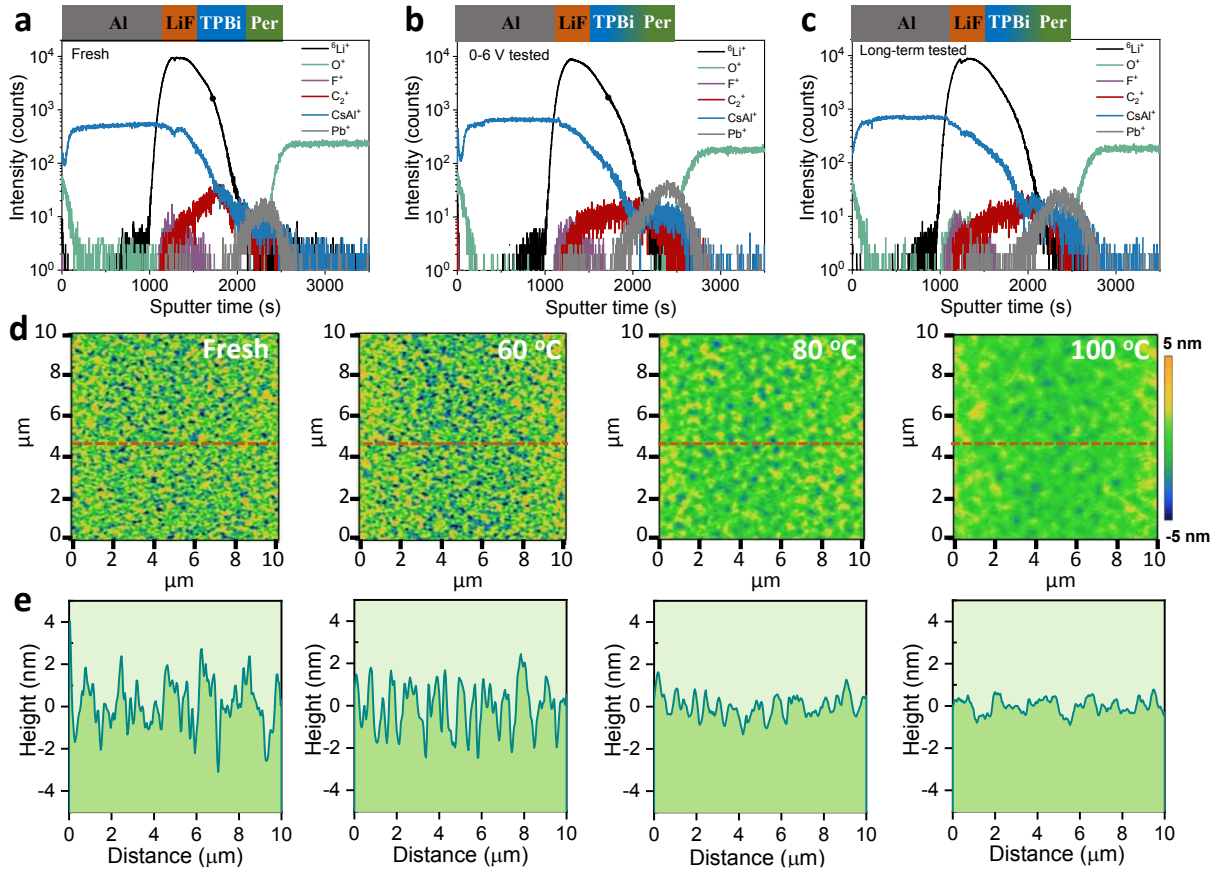

Fig. 3 Joule heating effects on the perovskite and TPBi surface. ToF-SIMS depth profile show the vertical element distribution of LEDs, (a) fresh, (b) scanned from 0 to 6 V, (c) after operational long-term stability test with luminescence decay to 30% of initial value. (d) AFM height topography image of TPBi films on the perovskite films under different annealing temperature of 30 °C (fresh), 60 °C, 80 °C and 100 °C. (e) Corresponding cross-section of profile in AFM height images.

To understand the origin of the observed interface degradation in the PeLEDs with the p-i-n device structure, we characterize thermal stability of the TPBi layer. In Fig. 3d and e, we show the atomic force microscopy (AFM) height images of TPBi layers deposited on perovskite films before and after thermal annealing at different temperature for 5 min. The TPBi without annealing show a root mean square (RMS) of 2.2 nm. We observe decreased surface roughness of the TPBi films after thermal annealing, exhibiting a reduced RMS of 0.6 nm after thermal annealing at 100 °C. We note that the morphology change is possibly due to the intrinsic thermal instability of TPBi attempt to explore possible strategies to mitigate the interfacial PL quenching through tailoring the device structures and/or reducing the Joule heating in the devices. We first try to suppress the element inter-diffusion through inserting a chemical inert aluminum oxide (Al_2O_3) thin layer deposited from atomic layer deposition (ALD) technique at the TPBi interfaces. Although we found suppressed PL quenching of perovskite layers under high temperature, the additionally incorporated insulating Al_2O_3 layer may deteriorates the electron injection efficiency in the devices, resulting in lower device performance of the obtained PeLEDs (Fig. S7). Alternatively, we attempt to

View Article Online
DOI: 10.1039/D0TC03816D

reduce the Joule heating in the complete device by improving the electric properties of the perovskite emissive layers. Based on our previous optimization strategy[43], we replaced the PEABr with an inorganic compound of LiBr, resulting in PeLED with a maximum luminance over 45,000 cd m^{-2} and a peak EQE of 15.3% (Fig. 4a and 4b). Moreover, owing to the improved electric properties of the perovskite emissive layer, the LiBr-based device exhibits obviously suppressed Joule heating during device operation (Fig. 4c). As a result, we achieved PeLEDs with an operational lifetime of 93 min at an initial luminescence of 1200 cd m^{-2} (Fig. 4d).

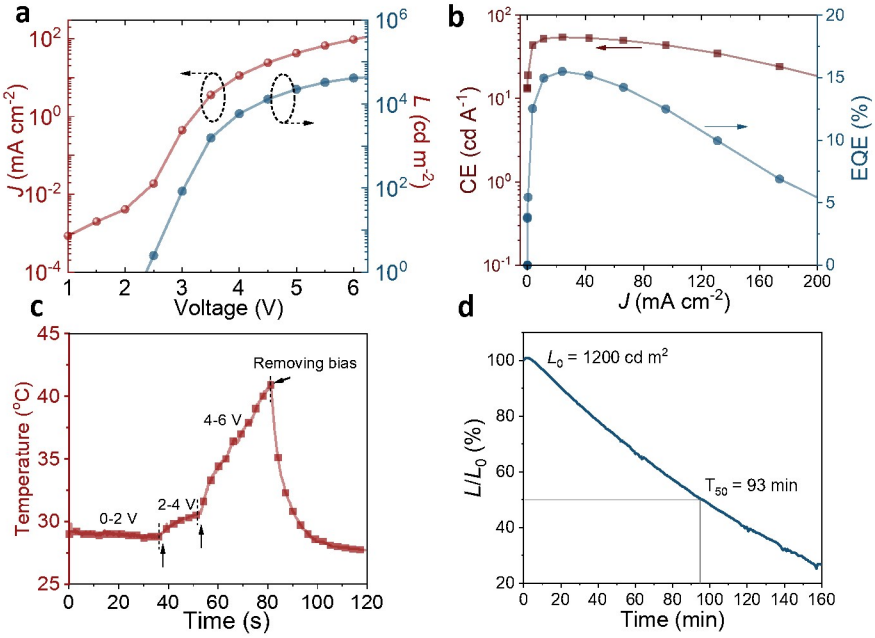

Fig. 4 Device performance of a LiBr-based PeLED. (a) *J-V-L* curve. (b) *CE-J-EQE* curve. (c) Temperature evolution of LiBr-based device scanned from 0 to 6 V. (d) Operational stability of LiBr-based device with initial luminescence of 1200 cd m^{-2}. The PeLEDs were tested in ambient (temperature, 30 °C; humidity, 60%) with epoxy encapsulation.

Conclusions

In this work, we clearly demonstrated the detrimental effects of interface degradation on the stability of PeLEDs. We revealed easy degradation of the charge transport interface between perovskite emissive layer and the commonly used electron transport layer of TPBi during device operation. The morphology evolution of thermally unstable TPBi induced by Joule heating causes direct contact or undesirable element inter-diffusion between the reactive Al electrodes and the perovskite films, resulting in significant PL quenching of the perovskite emissive layers and fast degradation of the PeLEDs. We demonstrated the possibility of partially overcoming the thermal-induced interface degradation of PeLEDs by improving the electric properties of the perovskite emissive layers. The presented results on device degradation mechanism of the interfacial contacts provide insightful information for further optimization of the perovskite emissive layers and the device structures toward PeLEDs with long-term operational stability. We suggest that further research efforts on improving the operational stability of PeLEDs lie in combined efforts on both reducing the Joule heating and constructing stable interfacial contacts between perovskites and the CTLs.

Experimental Section

PEABr synthesis: PEABr were synthesized by a widely reported method[34]. In detail, 6.71 g hydrobromic acid (Alfa, 48% in water) was added into ethanol solution containing 39.8 mmol phenethylamine (Acros, 99%) and vigorously stirring at 0 °C for 2 h. The obtained white powder was purified by ethanol and repeat two times. Then the products were dried at 50 °C for further purification.

Preparation of perovskite solutions: 0.2 mmol CsBr (Sigma Aldrich, 99.999%), 0.2 mmol $PbBr_2$ (Alfa, 99.999%), 0.08 mmol as-synthesized PEABr or 0.04 mmol LiBr, and 4 mg 18-Crown-6 (Sigma Aldrich, 99.99%) were dissolved in 1 mL DMSO (Acros, 99.999%) to form perovskite precursor solutions.

Device fabrication: The PeLEDs were fabricated on pre-patterned ITO glass substrates. Firstly, the ITO substrates were cleaned in acetone, ethanol and deionized water for 15 min in sequence, followed by ozone plasma treatment for 20 min before transferred into a glove-box (H_2O < 0.01 ppm, O_2 < 0.01 ppm) to deposit hole transport layer and perovskite emissive layer. The hole transport layer of PVK (Sigma Aldrich, 6 mg mL^{-1}

View Article Online
DOI: 10.1039/D0TC03816D

in chlorobenzene) was spin-coated on ITO glass at 4000 rpm, followed by thermal heating at 150 °C for 30 min. Then the perovskite precursor solution was spin-coated at 500 rpm for 5 s, and 3000 rpm for 55 s. The deposited perovskite films were annealed at 100 °C for 1 min. To complete the device fabrication, the devices were transferred into a thermal vacuum evaporator (base pressure below 2×10^{-6} mbar) to sequentially deposit approximately 20 nm TPBi (Hanfeng Chemical Co.) or 35 nm B3PYMPM, 1.5 nm LiF (Alfa), and 100 nm Al. The deposition rate for TPBi, B3PYMPM, LiF, and Al are approximately 0.4, 0.5, 0.2, and 2.0 Å s^{-1}, respectively. In the case of PeLEDs with ALD deposited Al_2O_3, after deposition of TPBi, the PeLEDs were moved into a chamber, where water molecule and trimethylaluminum (TMA) were utilized to form Al_2O_3. The thickness of each ALD cycle is approximately 0.102 nm. Finally, the fabricated devices were sealed by ultraviolet-curable resin before testing.

Characterizations: The surface temperature of PeLEDs was recorded with a near-infrared camera. A fluorescence spectrophotometer (HORIB-FM-2015) was used to acquire PL decay lifetimes of perovskite film. PL spectra were carried out by fluorescence spectrophotometer (HORIBA FL3). The digital photographs of perovskite films were taken by a smartphone. The GIXRD was measured by Shanghai Synchrotron Radiation Facility (SSRF) SSRF (Beamline 14). Due to the Al electrode on top of the perovskite films, we stripped the Al electrode away before the GIXRD measurement. AFM of TPBi films were acquired by in tapping mode with an Asylum Research Cypher S AFM microscope. The *J-V-L* characteristics, EL spectra, and operated lifetime of LEDs were obtained by a Keithley 2400 sourcemeter coupled with a PhotoResearch spectrometer PR670. Compositional depth profiling of perovskite films was carried out using a ToF-SIMS 5 system from IONTOF.

Conflicts of interest

There are no conflicts to declare.

Acknowledgements

This work was supported by the National Natural Science Foundation of China (91833303, 61974098, and 61674108), the National Key Research and Development Program (2016YFA0201900), the Priority Academic Program Development of Jiangsu Higher Education Institutions, the 111 program and Collaborative Innovation Center of Suzhou Nano Science and Technology (NANO-CIC). The work at Linköpoing is financially supported by the ERC Starting Grant (No. 717026) and the Swedish Energy Agency Energimyndigheten (No. 48758-1) F.F acknowledges the funding from the Swiss National Science Foundation (SNF)-Bridge POWER (project No.: 20B2-1_176552/1). Z.Y.T also thanks to Postgraduate Research & Practice Innovation Program of Jiangsu Province (KYCX18_2504) and financial support from China Scholarship Council (No. 201806920071).

References

1. Z.-K. Tan, R. S. Moghaddam, M. L. Lai, P. Docampo, R. Higler, F. Deschler, M. Price, A. Sadhanala, L. M. Pazos, D. Credgington, F. Hanusch, T. Bein, H. J. Snaith and R. H. Friend, *Nat. Nanotechnol.*, 2014, **9**, 687-692.
2. J. Song, J. Li, X. Li, L. Xu, Y. Dong and H. Zeng, *Adv. Mater.*, 2015, **27**, 7162-7167.
3. M. Yuan, L. N. Quan, R. Comin, G. Walters, R. Sabatini, O. Voznyy, S. Hoogland, Y. Zhao, E. M. Beauregard and P. Kanjanaboos, *Nat. Nanotechnol.*, 2016, **11**, 872-877.
4. H. Cho, S.-H. Jeong, M.-H. Park, Y.-H. Kim, C. Wolf, C.-L. Lee, J. H. Heo, A. Sadhanala, N. Myoung and S. Yoo, *Science*, 2015, **350**, 1222-1225.
5. Z. Xiao, R. A. Kerner, L. Zhao, N. L. Tran, K. M. Lee, T.-W. Koh, G. D. Scholes and B. P. Rand, *Nat. Photonics*, 2017, **11**, 108.
6. N. Wang, L. Cheng, R. Ge, S. Zhang, Y. Miao, W. Zou, C. Yi, Y. Sun, Y. Cao, R. Yang, Y. Wei, Q. Guo, Y. Ke, M. Yu, Y. Jin, Y. Liu, Q. Ding, D. Di, L. Yang, G. Xing, H. Tian, C. Jin, F. Gao, R. H. Friend, J. Wang and W. Huang, *Nat. Photonics*, 2016, **10**, 699-704.
7. Y. Cao, N. Wang, H. Tian, J. Guo, Y. Wei, H. Chen, Y. Miao, W. Zou, K. Pan and Y. He, *Nature*, 2018, **562**, 249-253.
8. K. Lin, J. Xing, L. N. Quan, F. P. G. de Arquer, X. Gong, J. Lu, L. Xie, W. Zhao, D. Zhang and C. Yan, *Nature*, 2018, **562**, 245-248.
9. T. Chiba, Y. Hayashi, H. Ebe, K. Hoshi, J. Sato, S. Sato, Y.-J. Pu, S. Ohisa and J. Kido, *Nat. Photonics*, 2018, **12**, 681-687.
10. W. Xu, Q. Hu, S. Bai, C. Bao, Y. Miao, Z. Yuan, T. Borzda, A. J. Barker, E. Tyukalova and Z. Hu, *Nat. Photonics*, 2019, **13**, 418-424.
11. X. Dai, Z. Zhang, Y. Jin, Y. Niu, H. Cao, X. Liang, L. Chen, J. Wang and X. Peng, *Nature*, 2014, **515**, 96-99.
12. H. Uoyama, K. Goushi, K. Shizu, H. Nomura and C. Adachi, *Nature*, 2012, **492**, 234-238.
13. Y. Liu, J. Cui, K. Du, H. Tian, Z. He, Q. Zhou, Z. Yang, Y. Deng, D. Chen and X. Zuo, *Nat. Photonics*, 2019, **13**, 760-764.
14. L. Na Quan, D. Ma, Y. Zhao, O. Voznyy, H. Yuan, E. Bladt, J. Pan, F. P. García de Arquer, R. Sabatini, Z. Piontkowski, A.-H. Emwas, P. Todorović, R. Quintero-Bermudez, G. Walters, J. Z. Fan, M. Liu, H. Tan, M. I. Saidaminov, L. Gao, Y. Li, D. H. Anjum, N. Wei, J. Tang, D. W. McCamant, M. B. J. Roeffaers, S. Bals, J. Hofkens, O. M. Bakr, Z.-H. Lu and E. H. Sargent, *Nat. Commun.*, 2020, **11**, 170.
15. H. Cho, Y. H. Kim, C. Wolf, H. D. Lee and T. W. Lee, *Adv. Mater.*, 2018, **30**, 1704587.
16. Y. Zou, Z. Yuan, S. Bai, F. Gao and B. Sun, *Mater. Today Nano*, 2019, 100028.
17. Z. Shi, S. Li, Y. Li, H. Ji, X. Li, D. Wu, T. Xu, Y. Chen, Y. Tian, Y. Zhang, C. Shan and G. Du, *ACS Nano*, 2018, **12**, 1462-1472.
18. Y. Miao, Y. Ke, N. Wang, W. Zou, M. Xu, Y. Cao, Y. Sun, R. Yang, Y. Wang, Y. Tong, W. Xu, L. Zhang, R. Li, J. Li, H. He, Y. Jin, F. Gao, W. Huang and J. Wang, *Nat. Commun.*, 2019, **10**, 3624.
19. Y. Yuan and J. Huang, *Accounts Chem. Res.*, 2016, **49**, 286-293.
20. S. Bai, P. Da, C. Li, Z. Wang, Z. Yuan, F. Fu, M. Kawecki, X. Liu, N. Sakai, J. T.-W. Wang, S. Huettner, S. Buecheler, M. Fahlman, F. Gao and H. J. Snaith, *Nature*, 2019, **571**, 245-250.

View Article Online
DOI: 10.1039/D0TC03816D

21. Y. Shao, Y. Fang, T. Li, Q. Wang, Q. Dong, Y. Deng, Y. Yuan, H. Wei, M. Wang, A. Gruverman, J. Shield and J. Huang, *Energy Environ. Sci.*, 2016, **9**, 1752-1759.
22. P. Vashishtha and J. E. Halpert, *Chem. Mater.*, 2017, **29**, 5965-5973.
23. H. Kim, L. Zhao, J. S. Price, A. J. Grede, K. Roh, A. N. Brigeman, M. Lopez, B. P. Rand and N. C. Giebink, *Nat. Commun.*, 2018, **9**, 4893.
24. Y. Shang, Y. Liao, Q. Wei, Z. Wang, B. Xiang, Y. Ke, W. Liu and Z. Ning, *Sci. Adv.*, 2019, **5**, eaaw8072.
25. T.-H. Han, J.-W. Lee, Y. J. Choi, C. Choi, S. Tan, S.-J. Lee, Y. Zhao, Y. Huang, D. Kim and Y. Yang, *Adv. Mater.*, 2020, **32**, 1905674.
26. H. Tsai, W. Nie, J. C. Blancon, C. C. Stoumpos, C. M. M. Soe, J. Yoo, J. Crochet, S. Tretiak, J. Even and A. Sadhanala, *Adv. Mater.*, 2018, **30**, 1704217.
27. Q. Dong, L. Lei, J. Mendes and F. So, *Journal of Physics: Materials*, 2020, **3**, 012002.
28. L. Zhao, K. M. Lee, K. Roh, S. U. Z. Khan and B. P. Rand, *Adv. Mater.*, 2019, **31**, 1805836.
29. L. Zhao, K. Roh, S. Kacmoli, K. Al Kurdi, S. Jhulki, S. Barlow, S. R. Marder, C. Gmachl and B. P. Rand, *Adv. Mater.*, 2020, **32**, 2000752.
30. C. Zou, Y. Liu, D. S. Ginger and L. Y. Lin, *ACS Nano*, 2020, **14**, 6076-6086.
31. K.-S. Cho, E. K. Lee, W.-J. Joo, E. Jang, T.-H. Kim, S. J. Lee, S.-J. Kwon, J. Y. Han, B.-K. Kim, B. L. Choi and J. M. Kim, *Nat. Photonics*, 2009, **3**, 341-345.
32. J.-M. Caruge, J. E. Halpert, V. Bulović and M. G. Bawendi, *Nano Lett.*, 2006, **6**, 2991-2994.
33. L. Zhang, F. Yuan, J. Xi, B. Jiao, H. Dong, J. Li and Z. J. A. F. M. Wu, *Adv. Funct. Mater.*, 2020, 2001834.
34. M. Ban, Y. Zou, J. P. H. Rivett, Y. Yang, T. H. Thomas, Y. Tan, T. Song, X. Gao, D. Credgington, F. Deschler, H. Sirringhaus and B. Sun, *Nat. Commun.*, 2018, **9**, 3892.
35. X. Yang, X. Zhang, J. Deng, Z. Chu, Q. Jiang, J. Meng, P. Wang, L. Zhang, Z. Yin and J. You, *Nat. Commun.*, 2018, **9**, 570.
36. J. Song, T. Fang, J. Li, L. Xu, F. Zhang, B. Han, Q. Shan and H. Zeng, *Adv. Mater.*, 2018, **30**, 1805409.
37. V. González-Pedro, S. A. Veldhuis, R. Begum, M. J. Bañuls, A. Bruno, N. Mathews, S. Mhaisalkar and A. n. Maquieira, *ACS Energy Lett.*, 2018, **3**, 1409-1414.
38. S. Chung, J.-H. Lee, J. Jeong, J.-J. Kim and Y. Hong, *Appl. Phys. Lett.*, 2009, **94**, 253302.
39. P. Tyagi, L. Indu Giri, S. Tuli and R. Srivastava, *J. Appl. Phys.*, 2014, **115**, 034518.
40. J. H. Kwon, S. Choi, Y. Jeon, H. Kim, K. S. Chang and K. C. Choi, *Appl. Mater. Interfaces*, 2017, **9**, 27062-27072.
41. L. Zhao, R. A. Kerner, Z. Xiao, Y. L. Lin, K. M. Lee, J. Schwartz and B. P. Rand, *ACS Energy Lett.*, 2016, **1**, 595-602.
42. N. Li, L. Song, Y. Jia, Y. Dong, F. Xie, L. Wang, S. Tao and N. Zhao, *Adv. Mater.*, 2020, 1907786.
43. T. Wu, J. Li, Y. Zou, H. Xu, K. Wen, S. Wan, S. Bai, T. Song, J. A. McLeod, S. Duhm, F. Gao and B. Sun, *Angew. Chem. Int. Ed.*, 2020, **59**, 4099-4105.